Quantitative Theories of Metacontrast Masking

Gregory Francis
Purdue University, Department of Psychological Sciences

In metacontrast masking, the effect of a visual mask stimulus on the perceptual strength of a target stimulus varies with the stimulus onset asynchrony (SOA) between them. As SOA increases, the target percept first becomes weaker, bottoms out at an intermediate SOA, and then increases for still larger SOAs. As a result, a plot of target percept strength against SOA produces a u-shaped masking curve. A variety of theories have proposed special mechanisms to account for this u-shaped masking curve, but new mathematical analyses indicate that the u-shaped masking curve is a robust characteristic of a large class of neurally plausible systems. Three quantitative methods of accounting for the u-shaped masking effect are described; then four previously published mathematical models of masking are analyzed. All the models are shown to produce the u-shaped masking curve with a common method, called mask-blocking, whereby a strong internal representation of the target blocks the mask's effects.

This formatted manuscript was created by the author and does not correspond exactly to the manuscript published in the journal. References to page numbers should refer to the published article.

Introduction

The percept of a briefly flashed visual target is often weakened when it is followed by a masking stimulus. If the target and mask have equal intensities and duration, and the target is a filled circle and the mask is an annulus surrounding the circle, then the mask often has its biggest effect when it is delayed relative to the target. It is common in these types of experiments to plot a measure of the target's perceptual strength as a function of interstimulus interval (ISI) or stimulus onset asynchrony (SOA), as is shown in Figure 1 (Francis, 1998). This masking curve takes a u-shape, indicating that the mask has its biggest effect for intermediate values of SOA or ISI. The effect of the mask is sometimes referred to as an "inverted-u" effect, which would be drawn if one plotted the effectiveness of the mask as a function of ISI or SOA. This type of masking is called metacontrast masking, and it has been widely studied, with the u-shaped masking curve playing a prominent role (e.g., Alpern, 1953; Bachmann, 1994; Breitmeyer, 1984; Breitmeyer & Ganz, 1976; Kahneman, 1967; Lefton, 1973; Reeves, 1982; Weisstein, 1972).

Soon after the computing technology was available, vision scientists developed computational models that produced a u-shape in metacontrast masking conditions (Weisstein, 1968; Bridgeman, 1971), an approach that continues today (Anbar & Anbar, 1982; Francis, 1997). While these models have individually attempted to unify a variety of data on visual masking, and metacontrast masking in particular, there has been little effort to unify the models themselves. This manuscript compares and contrasts the different models and identifies underlying themes common to all the models. As part of this analysis, it was noted that occasionally the original description of a model did not accurately portray its account of masking.

The quantitative basis of the u-shaped metacontrast masking curve is analyzed in two ways. First, three methods of producing the u-shaped curve are introduced in the context of a fairly general mathematical system. One method, called *efficient masking*, is proven to robustly produce the u-shaped masking curve for this system. The other two methods, called *mask-blocking* and *target-blocking* are more qualitative methods, with their properties demonstrated by computer simulation. Second, existing quantitative models of metacontrast masking are analyzed to identify how the three methods are utilized by the different models. The main findings are: (1) no model uses efficient masking, (2) all of the models use mask-blocking, and (3) only one model uses target-blocking. One conclusion from this analysis is that the u-shaped masking curve is a natural and robust property of a variety of models, including models that have not previously been analyzed under metacontrast masking conditions.

Quantitative methods of masking

This section describes three methods of producing a u-shaped masking curve under metacontrast conditions. The goal here is to identify the quantitative underpinnings of the u-shaped masking curve by analyzing mathematical systems without regard to any particular model. In the next section the quantitative analysis started here will be applied to specific models of metacontrast masking.

To demonstrate the methods, a common mathematical sys-

*Correspondence concerning this article should be addressed to Gregory Francis, Department of Psychological Sciences, 1364 Psychological Sciences Building, Purdue University, West Lafayette, Indiana 47907-1364. Electronic mail may be sent to gfrancis@psych.purdue.edu.

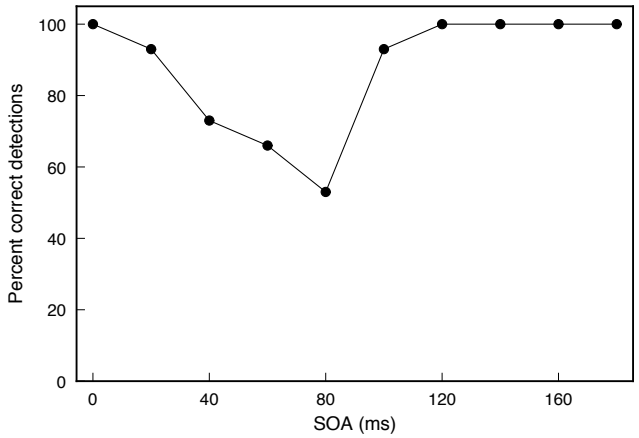

Figure 1: Typical results from a metacontrast masking experiment demonstrate the u-shaped masking curve. In this detection experiment the percentage of correct detections of the target first decreases then increases as the SOA between the target and mask increases. See Francis (1998) for details of the experiment.

tem will be used. Let $x(t)$ correspond to a visual response function (VRF) produced by the visual system in response to a target stimulus. Describe $x(t)$ by a differential equation of the following sort:

$$\frac{dx}{dt} = -Ax + (B - Cx)I(t) - (D + Ex)J(t), \tag{1}$$

where A, B, C, D, and E are non-negative parameters, and where $I(t)$ and $J(t)$ correspond to target and mask signals, respectively. This equation is not intended to necessarily be a model of any part of the visual system, but variations of this type of equation have been used extensively in the neural network literature, where it would be called a shunting equation (e.g., Grossberg, 1983).

To gain insight into the behavior of equation (1), consider the behavior of $x(t)$ under metacontrast conditions. Define the target, $I(t)$, and mask, $J(t)$, terms in equation (1) as:

$$I(t) = \begin{cases} I & \text{for } 0 \le t < \tau_1 \\ 0 & \text{otherwise,} \end{cases} \tag{2}$$

and

$$J(t) = \begin{cases} J & \text{for } \tau_1 + \tau_2 \le t < \tau_1 + \tau_2 + \tau_3 \\ 0 & \text{otherwise.} \end{cases} \tag{3}$$

Here, time zero corresponds to onset of the target, τ_1 corresponds to the duration of the target, τ_2 corresponds to the ISI duration between offset of the target and onset of the mask, and τ_3 corresponds to the duration of the mask. When the target is present, $x(t)$ grows toward the value $BI/(A + CI)$ at a rate set by $(A + CI)$. During a positive ISI, $x(t)$ undergoes passive decay toward the value zero at a rate set by A. When the mask is present, $x(t)$ decreases toward the value $-DJ/(A + EJ)$ at a rate set by $(A + EJ)$. After mask offset, $x(t)$ again decays toward the value zero at a rate set by A. The system is piecewise linear, and an analytic solution is given in the appendix (Theorem 1).

Assume that the perceptual strength, P, on which a person bases a judgment in an experimental task (e.g., detection, identification, brightness match) is related to an integration of a function of the VRF:

$$P = \int_0^T F[x(t)]dt, \tag{4}$$

where $F[\ ]$ is a properly chosen function, and T is the stopping time of the integration. The choices of $F[\ ]$ and T correspond to different assumptions about the relationship of the VRF to the visual percept, as discussed in detail below.

The following analysis considers three special cases of equations (1)–(4) that produce the u-shaped masking curve. It should be emphasized that this analysis is not proposing models of metacontrast masking, but is only analyzing mathematical systems that produce a u-shaped masking curve. Inherently some of the mathematical systems will imply certain types of models, but the connection of the mathematical systems to models is postponed until the next section.

Efficient masking

The first method of producing the u-shaped masking curves is called *efficient masking* because the mask has its biggest effect on the target VRF (is more efficient) when it is presented later rather than sooner. For this approach, suppose that longer durations of the VRF correspond to stronger percepts. This relationship is consistent with theories of consciousness that assume neural signals must resonate or persist for substantial lengths of time for responses to be based on them (Grossberg, 1980, 1999; Dennett, 1992). Equation (4) measures the total time $x(t)$ is above a threshold if

$$F[x] = \begin{cases} 1 & \text{for } x > G \\ 0 & \text{otherwise,} \end{cases} \tag{5}$$

where G is a non-negative threshold parameter and T in equation (4) is set large enough that the integral considers all nonzero values of $F[x]$.

To relate equations (1)–(5) to metacontrast masking, values of P are measured for different ISIs between the target and the mask stimuli. A notable finding is that this system produces the u-shaped masking curve in a very robust manner, provided that the VRF outlasts the mask signals. Intuitively, the persisting VRF of the target will last for a duration that depends on both the inherent rate of decay of the VRF and the effect of the mask. During the ISI, the change in the VRF ($-Ax$) depends on the value of the VRF itself, so that just after offset of the target input, the VRF undergoes rapid decay. As the VRF decreases in value, the change in the VRF decreases. The effect of the mask is to decrease the VRF, and this decrease also has an effect on the rate of VRF decay. The mask is most efficient if the VRF is left alone during its rapid decay period and the mask arrives during the slow decay period. The mask is less efficient if its effect co-occurs with the rapid decay period because it leads to still slower decay after the mask has turned off.

For those readers familiar with the mathematics of cooling surfaces the following analogy may help. Suppose you have a

too hot cup of coffee and you want the coffee to reach a lesser temperature as quickly as possible by adding a small container of refrigerated cream. Suppose that the cream is not so cold that adding it immediately will bring the coffee to the desired temperature. Then with application of Newton's law of cooling (and assuming convection, stirring of the coffee, insulated sides of the cup, etc.) one finds that the cream is most effective when it is added after a delay. The reasoning is exactly as above; adding the cream early cools the coffee at a time when there would otherwise be substantial cooling, with or without the cream. Adding the cream a bit later allows the natural cooling of the coffee to occur unperturbed and then still allows for the direct cooling effect of the cream. This effect is the basis of a comment in Gardner (1961, p. 145), where a colleague tells him, "If you want to keep your coffee hot,...better pour your cream now instead of later. The hotter the coffee, the faster its rate of heat loss." The cream is less efficient at cooling the coffee when added earlier, analogous to the effect of the mask in metacontrast masking. Indeed, when equations are written to describe the coffee cooling problem, one finds that a subset of these equations is isomorphic to a subset of equations (1)-(5).

The following theorem (proven in the appendix) shows the conditions where increases in ISI lead to decreases in P. This relationship produces the downward slope of the u-shaped masking curve.

Theorem 1: Efficient masking.

Let the VRF and percept strength be defined as in equations (1), (4) and (5), with $x(0) = 0$. Let the target and mask terms be defined as in equations (2) and (3), respectively. Choose parameters so that $D > 0$, $J > 0$, $\tau_2 \geq 0$, and $x(\tau_1+\tau_2+\tau_3) > G$, which implies that the VRF is above threshold at the offset of the mask. Set T in equation (4) large enough so that the integral includes all non-zero terms of $F[x(t)]$. Then

$$\frac{\partial P}{\partial \tau_2} < 0,$$

which means that increases in ISI correspond to smaller P values and weaker percepts.

Theorem 1 demonstrates that many systems defined by equations (1)-(5) produce an increase in masking strength as ISI increases. This result is extremely robust, as the theorem conditions can be satisfied with a variety of parameter choices.

Efficient masking produces the u-shaped masking curve because of the interaction of the target VRF decay function and the mask signal. Presenting the mask early undermines the effectiveness of the natural decay function. Delaying the mask allows the rapid natural decay to occur and then be followed by the direct effect of the mask signal. Delaying the presentation of the mask too long allows the target VRF to decay so much that the mask has a diminished effect that grows smaller with further increases in ISI.

Theorem 1's requirement that the mask be unable to drive the VRF below threshold is of critical importance. When $x(\tau_1 + \tau_2 + \tau_3) \leq G$, an increase in ISI either increases P (the inhibition comes later and the VRF vanishes later) or has no effect (the VRF vanishes before the mask appears). As a result, the strongest masking occurs when the VRF reaches its threshold at exactly the same time that the mask signal ends. This observation leads to the following lemma.

Lemma 1: Most effective ISI.

For the system defined in Theorem 1 with varying τ_2 and otherwise fixed parameters, the ISI that produces the strongest masking, designated as τ_2^*, is:

$$\tau_2^* = \frac{1}{A} \ln \left\{ \frac{BI}{A+CI} \left(1 - e^{-(A+CI)\tau_1}\right) \right\} -$$

$$\frac{1}{A} \ln \left\{ G + \frac{DJ}{A+EJ} \left(1 - e^{-(A+EJ)\tau_3}\right) \right\} - \frac{A+EJ}{A}\tau_3. \quad (6)$$

This result is found by setting $x(\tau_1 + \tau_2^* + \tau_3) = G$, which says that the VRF reaches threshold at the end of the mask signal, and solving for τ_2^*. The proof is in the appendix.

Figure 2A shows a masking curve based on equations (1)–(5) for one set of parameters. The parameters have been chosen to highlight properties of the system rather than to match any experimental data. Details of the calculations are given in the appendix. The stimulus duration was 20 milliseconds, so Theorem 1 applies for SOA$\geq$ 20. Figure 2A shows that the duration of $x(t)$, P, decreases as SOA increases up to 100 milliseconds. Figure 2B plots $x(t)$ for four SOAs. The curves for SOA=20 and SOA=80 are applicable to Theorem 1. As the figure shows, the application of the mask's signal at time 20 or 80 results in a drop in $x(t)$. However, the reduction is such that at time 100, when the mask has just ended for the SOA=80 condition, the SOA=80 curve is below the SOA=20 curve. That is, adding the inhibition later leads to a smaller $x(t)$ value after mask offset. Since $x(t)$ simply undergoes exponential decay beyond time 100, the later mask produces a shorter $x(t)$ duration. Once the SOA increases beyond $\tau_1 + \tau_2^*$ (100 milliseconds for the given parameters), the duration of the VRF increases an amount that corresponds to the increase in SOA, thus the straight line increase for SOAs beyond 100 in Figure 2A, until the VRF disappears before the mask appears at SOAs beyond 180.

Efficient masking also accounts for a number of other properties of metacontrast masking. For example, the ISI for which the strongest masking occurs is known to shift to smaller values (and the masking curve to become monotonically increasing from zero) as mask intensity and duration increases (Weisstein, 1972; Breitmeyer, 1978). This is also a property of any system that satisfies the conditions in Theorem 1 because a stronger mask more quickly pulls the VRF down to the threshold value. This effect is quantified by noting that

$$\frac{\partial \tau_2^*}{\partial J} < 0, \quad (7)$$

which says that the strongest masking occurs for smaller ISIs as the mask signal increases in intensity. A similar lemma shows that

$$\frac{\partial \tau_2^*}{\partial \tau_3} < 0, \quad (8)$$

which indicates that the strongest masking occurs for smaller ISIs as the mask signal increases in duration. These results are

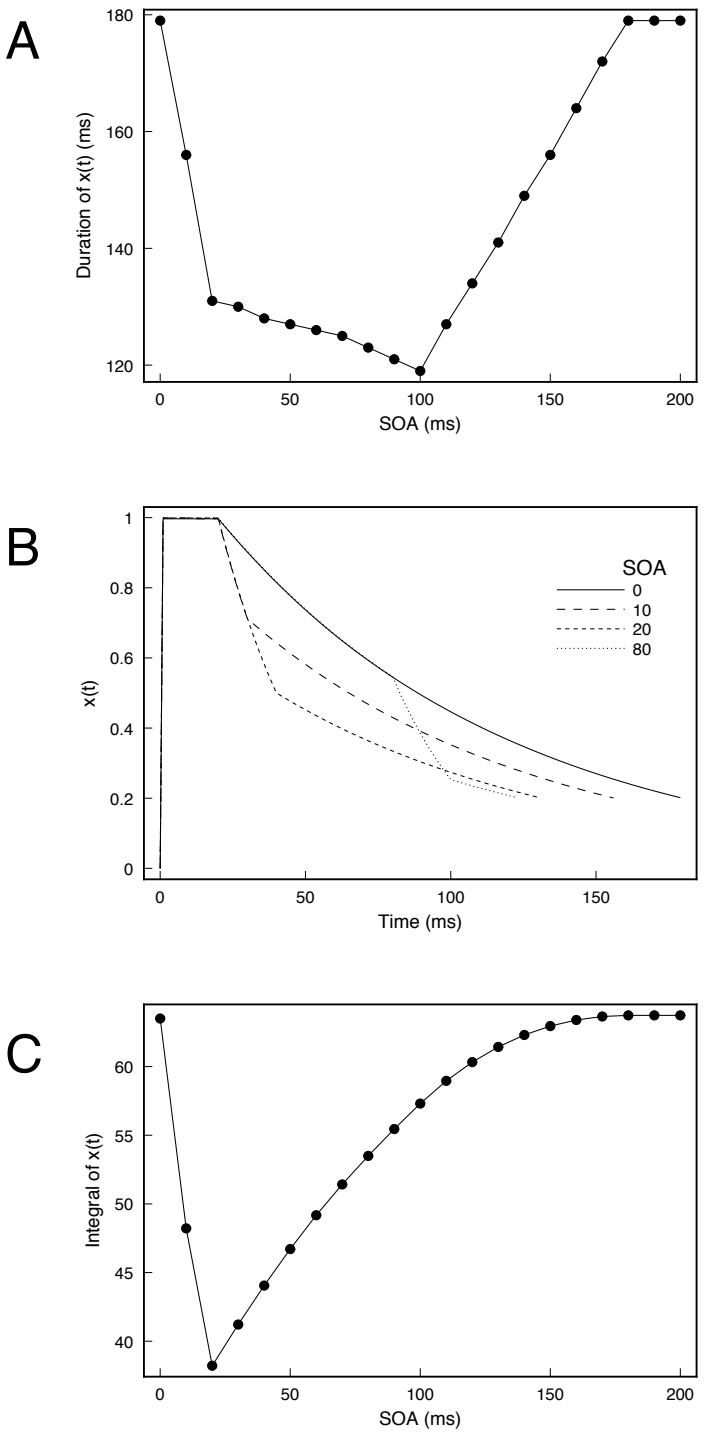

Figure 2: Simulation results based on equations (1)–(4) with parameters chosen to show effects of efficient masking and mask-blocking. A shows a u-shaped masking curve based on efficient masking. B plots $x(t)$ for four different SOAs. C shows a u-shaped masking curve based on mask-blocking.

proven as Lemmas 2 and 3 in the appendix. In each case, the basic effect is that the stronger mask has a bigger effect on the VRF, and so Theorem 1, with its requirement that the VRF persist beyond the offset of the mask, can only be satisfied for smaller ISI values. For masks strong enough to decrease the VRF below threshold before the mask disappears, Theorem 1 never applies.

None of the characteristics of efficient masking seem to be strongly dependent on the precise form of equations (1) to (5). For example, if $I(t)$ and $J(t)$ are not step functions but gradually turn on and off, the masking curves are similar, but more complicated to analyze. Likewise, Theorem 1 only considers times after target offset, so how the VRF activity is produced by the target is not important for the general result. This means that a variety of models with persisting responses that decay away are likely to show the u-shaped masking curve, if model parameters are set appropriately. This includes models of brightness perception (Hildreth, 1973); flicker detection (Sperling & Sondhi, 1968), visual persistence (Di Lollo & Bischof, 1995; Dixon & Di Lollo, 1994; Farrell, Pavel, & Sperling 1990; Francis, 1999), information extraction (Busey & Loftus, 1994; Loftus, Duncan & Gehrig, 1992), physiological visual systems (Gaudiano, 1992; Grossberg, 1983) and models explicitly designed to account for masking effects, as described below.

Applying Theorem 1 to these models does require a particular linking hypothesis between the model response and the strength of the visual percept. Theorem 1 proves the effect of efficient masking only when the relationship between the VRF and the quality of the target percept is linked by the *duration* of the VRF signal. If the relationship between the VRF and the quality of the percept is modified, the u-shaped masking curve may not appear. For example, if the *integral* of the VRF is assumed to be related to the percept, the u-shaped masking curve does not appear with increases in ISI. To be more specific, define the $F[x]$ function in equation (4) as returning that part of the VRF that is above a given threshold value:

$$F[x] = [x - G]^+, \tag{9}$$

where the notation $[\ ]^+$, indicates setting negative values equal to zero. Here G is again a non-negative threshold parameter and $F[\ ]$ simply passes along the remainders above this threshold. When this definition of $F[\ ]$ is combined with equations (2) and (3) for the target and mask signals, respectively, we get the following result, which is proven in the appendix.

Theorem 2.

Let the VRF and percept strength be defined as in equations (1), (4) and (9), with $\tau_2 \geq 0$, and $x(0) = 0$. Let the target and mask terms be defined as in equations (2) and (3). Set T in equation (4) large enough so that the integral includes all non-zero terms of $F[x(t)]$. Then

$$\frac{\partial P}{\partial \tau_2} \geq 0.$$

This means that increases in positive ISIs correspond to either larger or unchanging P, which implies monotonically decreasing masking strength. Thus, with percept strength linked to the

integral of the VRF, equations (1)–(4) cannot directly produce the u-shaped masking curve. This result is of special interest because most of the current models of metacontrast masking relate percept quality to an integral of a VRF, and this relationship precludes efficient masking from contributing to the u-shaped masking curve in those models. The next two sections explore two other general methods of producing a u-shaped masking curve: mask-blocking and target-blocking.

Mask-blocking

A second method of masking can also be described with equations (1)–(4). The target signal can block the effect of a relatively weak mask signal, thereby limiting the mask's effects to those SOAs where the target signal is weak.

As Figure 2A indicates, the strength of the target percept decreases for SOAs that would lead to negative ISI values (where Theorem 1 would not apply) and target and mask signals coexist for some duration. The basis of this effect is different from the effect of efficient masking. The mask signal in this system is relatively weak, which is necessary to satisfy the condition in Theorem 1 that the VRF persists beyond the offset of the mask signal. Thus, when both target and mask signals feed into equation (1), the target signal dominates the mask signal. The presence of the strong target signal drives $x(t)$ close to ceiling, thereby *blocking* the effect of the mask signal. When both target and mask are present, $x(t)$ approaches the limiting value

$$\frac{BI - DJ}{A + CI + EJ} \tag{10}$$

at a rate set by $A + CI + EJ$. In Figure 2 this rate was quite fast, due to the large value of CI. If parameters are set so that $BI >> DJ$ and $CI >> EJ$, then the limiting value is very close to what it would be without the mask. When the target turns off but the mask remains present, the limiting value changes to:

$$\frac{-DJ}{A + EJ}, \tag{11}$$

with the rate of approach set by $A + EJ$. In Figure 2, this rate was fairly slow, due to the small rate of passive decay, A, and the weak mask signal, EJ. In (11) $x(t)$ is not pushed to ceiling by a strong target signal, so the mask signal has a notable effect. Taken together, equations (10) and (11) show that the mask only has much of an impact on $x(t)$ when it appears without the target signal. As SOA increases, the mask signal is presented by itself for longer durations, thereby producing stronger masking. This effect is named *mask-blocking* because a strong target signal blocks the effect of the mask.

Figure 2B demonstrates mask-blocking by comparing SOA=0, SOA=10, and SOA=20 curves. For time less than 20 milliseconds, the SOA=20 curve (which has no mask signal before time 20) is essentially superimposed on the SOA=0 curve (which has a mask signal all times before time 20), because the strong target signal pushes $x(t)$ close to a ceiling value and the relatively weak signal from the mask in the SOA=0 condition cannot pull it down from the ceiling. Beyond time 20 milliseconds, the SOA=20 curve is much smaller than the SOA=0 curve, indicating the influence of the mask for the SOA=20 condition. As SOA increases from zero, the temporal overlap of the target and mask signals decreases, and the duration of the mask signal alone increases. The more the mask signal is presented by itself, the stronger the effect of the mask, as a comparison of the SOA=10 and SOA=20 curves demonstrates. This explains the drop in Figure 2A for changes in SOA from 0 to 20. Once the SOA increases enough that the mask signal is always presented by itself, mask-blocking no longer occurs but efficient masking occurs. This change in masking type is evident in Figure 2A at SOA=20, where the slope of the curve changes dramatically. Thus, the masking curve in Figure 2A actually shows two separate masking effects. Mask-blocking applies for SOAs less than 20 (negative ISIs) and efficient masking applies for SOAs greater than 20 (positive ISIs).

Notably, even when the strength of the percept is linked to the integral of the VRF, as in equation (9), mask-blocking can produce a u-shaped masking curve; albeit one with a severe limitation. If the mask signal has little effect when the target signal is also present, then increases in SOA allow the mask to inhibit more of the persisting response of the VRF. Thus, up until SOA increases to the duration of the target (and Theorem 2 applies), increases in SOA will lead to stronger masking. Figure 2C plots a masking curve that demonstrates mask-blocking with an integration-based linking hypothesis. Figure 2C is based on the same computations of $x(t)$ as in Figures 2A and B.

A limitation of the mask-blocking account of metacontrast masking is that it predicts a u-shaped masking curve when target percept strength is plotted against SOA, but not against ISI. If Figure 2C were replotted with ISI on the abscissa, the bottom of the curve would be at ISI=0. This property is inconsistent with many experimental studies, which often find that the strongest masking occurs for positive ISIs. To fix this discrepancy, a model that uses mask-blocking as the basis of the u-shaped masking curve needs to extend the target signal's blocking properties so that the mask has little effect even for some positive ISIs. Additional analysis, below, shows how various models of metacontrast masking implement this technique.

Target-blocking

A third method of producing the u-shaped masking curve can also be described with equations (1)–(4). In this method, called target-blocking, the effect of the mask is to prohibit or curtail the target signal's contribution to the VRF. As with mask-blocking, target-blocking cannot directly account for the u-shaped masking curve across positive ISIs. To fix this limitation, target-blocking requires that the signal from the target is delayed relative to the physical presence of the target itself.

Both efficient masking and mask-blocking presume, in different ways for each method, that the effect of the mask is weak. In contrast target-blocking occurs when the effect of the mask is so strong that the target signal has little opportunity to contribute to the calculation of a strong percept. Consider equations (10) and (11) again, but now suppose that the parameters no longer favor the target signal. If the target and mask signals are presented simultaneously, a strong mask signal may prohibit $x(t)$

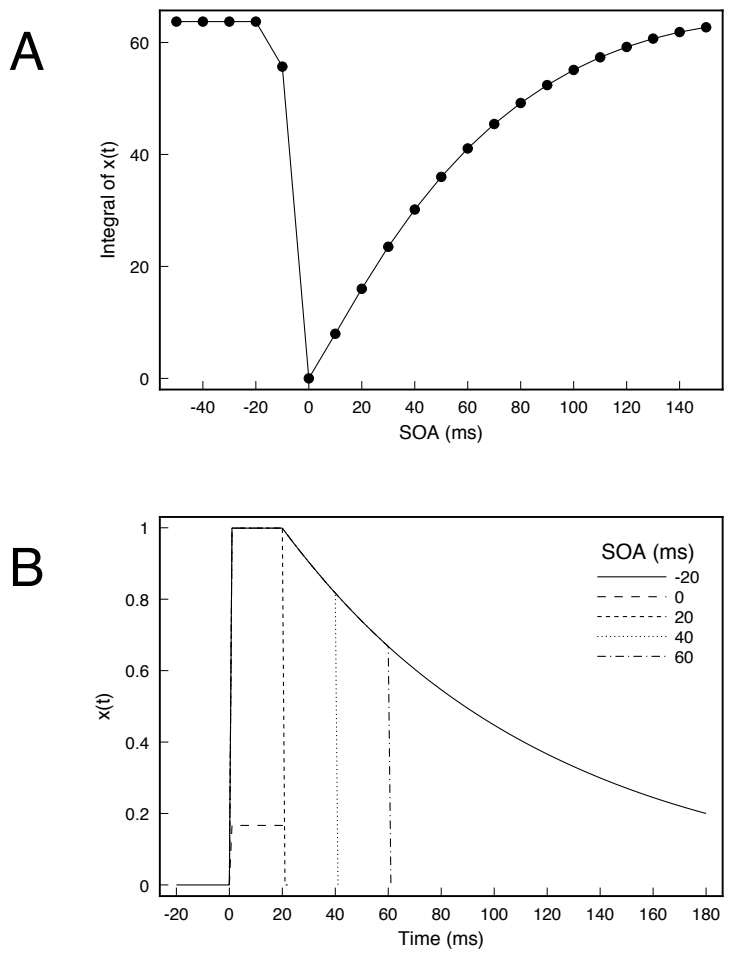

Figure 3: Simulation results based on equations (1)–(4) with parameters chosen to show effects of target-blocking. A shows a masking curve based on target-blocking. B plots $x(t)$ for different SOAs. For SOA=0, $x(t)$ never goes above the threshold of 0.2.

from ever reaching a very large value, and the corresponding percept strength will be small. When the mask signal follows the target signal, $x(t)$ may get quite large before the mask appears.

Equations (1)–(4), but with a different set of parameters, can demonstrate the effect of target-blocking, and results are plotted in Figure 3. Figure 3A plots the masking curve [using the integral of $x(t)$ as in equations (4)and (9)]. Because the effect of the mask is very strong, the target signal is blocked when the mask signal coexists with it, as for SOA=0, and $x(t)$ is greatly attenuated. For longer SOAs, the effect of the mask is to quickly curtail any remaining $x(t)$ value. Figure 3B plots $x(t)$ as a function of time for different SOAs. The mask has its strongest effect for SOA=0. When SOA=0, $x(t)$ never goes above threshold for integration (0.2), so the percept strength is zero. As SOA increases, the target signal does rise above the integration threshold, and the fading trace of $x(t)$ remains above threshold for longer durations, thereby leading to larger values in the calculation of percept strength.

Because the strongest masking always occurs for SOA=0, target-blocking cannot produce a proper u-shaped masking curve, with its minimum at a positive ISI, unless one assumes that the timing of the target signal is offset from the timing of the physical stimulus. In particular, suppose that the target signal, $I(t)$ in equation (1), is delayed by δ time units relative to the actual onset and offset of the physical target stimulus. If SOA is recalculated to reflect this delay, then the new SOA values will take values δ time units greater than before. Thus, the masking curve in Figure 3A will be shifted δ time units to the right, and will show a u-shaped masking curve with the lowest point at SOA=δ. More generally, both the target and mask signal may be delayed relative to their respective physical stimuli. As long as the target signal is delayed more than the mask signal, a u-shaped masking curve will be produced with the strongest masking at a positive ISI.

An example of target-blocking is the transient-sustained explanation of metacontrast masking (e.g., Breitmeyer & Ganz, 1976; Breitmeyer, 1984; Weisstein, 1968, 1972). In this theory the mask produces a strong and fast signal while the target produces a slower signal that is delayed relative to the mask's signal. The net effect is that the target and mask signals overlap the most, and the mask has its biggest effect, when there is a positive SOA between the physical stimuli.

Intermediate conclusions

This section has described three quantitative methods of producing the u-shaped masking curve. Of the three methods, efficient masking is, in one sense, the most straightforward, as it needs the fewest assumptions about the properties of the target and mask signals. It is somewhat surprising then, to discover that efficient masking seems to have never been considered as an explanation for the u-shaped masking curve.

On the other hand, both mask-blocking and target-blocking are less sensitive than efficient masking to the relationship between the VRF and percept strength. While efficient masking does not apply when the percept strength is related to the integral of the VRF, mask-blocking and target-blocking produce u-shaped masking curves for a wide variety of relationships. Mask-blocking and target-blocking are more qualitative descriptions of masking; but their properties can be instantiated in a variety of mathematical systems. Indeed, their properties have previously been recognized as methods of producing the u-shaped masking curve, although sometimes only in verbal theories that have not been converted to quantitative models.

The different methods can exist in isolation or can coexist. For example, the masking curve in Figure 2A shows effects of both efficient masking and mask-blocking. The former is demonstrated for SOAs greater than 20 (positive ISIs) while the latter occurs for SOAs less than 20 (negative ISIs). Likewise, if the mask signal has any effect on the VRF when it coexists with the target signal, some amount of target-blocking is possible, although any effects may be washed out by the larger effects of efficient masking or mask-blocking. This is the case for the masking curves in Figures 2A and C, where minuscule effects of target-blocking are below the resolution of the graph

in Figure 2B.

Target blocking can exist by itself, if the mask is so strong that no part of the VRF persists after the mask signal. In such a case neither efficient masking nor mask-blocking can occur. It is also possible to get mixtures of appreciable target-blocking and mask-blocking by varying mask strength. An example of this type of mixing is shown below.

Analysis of previous models

The discussion now turns to an analysis of earlier models of metacontrast masking. There are a great variety of theories of metacontrast masking, with particular interest in accounting for the u-shaped masking curve. Four of these theories have been described as quantitative models. In the subsequent analyses we summarize what part of each model is critical for producing its fundamental behavior and, in some cases show, that the original authors misunderstood key mechanisms of their model. The main finding is that all of the models use mask-blocking to produce the u-shaped masking curve.

All the models provide a quantitative description of masking, but for some models the current analysis relies on simulation examples rather than a mathematical description. The following discussion presents the models in order of how quantitatively the explanation of masking mechanisms can be described.

Anbar and Anbar's decay model

Anbar and Anbar (1982) proposed a connection between models of brightness perception (Hildreth, 1973) and the u-shaped metacontrast masking curve. Their approach was similar to the analysis of equation (1); they defined a visual response function and made some assumptions about how the mask interacts with the VRF. Using the earlier notation, the equation for the VRF generated by a target and followed by a mask is:

$$x(t) = \begin{cases} I & \text{for } 0 \le t < \tau_1 \\ Ie^{[-I^\gamma (t-\tau_1)]} & \text{for } \tau_1 \le t < \tau_1 + \tau_2 \\ Ie^{[-I^\gamma \tau_2]} \left(\frac{Ie^{[-I^\gamma \tau_2]}}{J} \right)^p & t = \tau_1 + \tau_2 \\ x(\tau_1+\tau_2) e^{[-x(\tau_1+\tau_2)^\gamma (t-\tau_1-\tau_2)]} & \text{for } t > \tau_1 + \tau_2, \end{cases} \quad (12)$$

where γ and p are parameters that are also used in models of spatial brightness contrast. As before, τ_1 is the target duration and τ_2 is the ISI between offset of the target and onset of the mask. The mask duration is not specified because in Anbar and Anbar's model it only has an effect on the target's VRF at its onset.

The first line of equation (12) sets $x(t)$ as the strength of the target input. The second line describes exponential decay at a rate determined by the strength of $x(t)$ at target offset, which is the value I. The third line describes a discontinuous drop in $x(t)$ at the onset of the mask. The effect of the mask is to drop $x(t)$ to a fraction of the value it would have were there no mask. The fraction is the ratio of the current value of $x(t)$, which is $I \exp[-I^\gamma \tau_2]$, and the value of the mask input, J. This ratio is the fraction in line three, and will be called the *masking ratio* in the discussion below. The masking ratio is raised to the power p before multiplying the current value of $x(t)$. The fourth line indicates exponential decay after the mask-induced drop, at a rate determined by the strength of the VRF at mask onset, $x(\tau_1 + \tau_2)$. The strength of the target percept, P, was modeled as the integral of $x(t)$ as in equations (4) and (9) with $G = 0$.

After an analysis similar in style to the proof of Theorem 1, Anbar and Anbar (1982) showed that the integral of $x(t)$, P, decreases as ISI increases, up to a maximum ISI. This produces the downward slope of the u-shaped masking curve. Beyond that maximum ISI, further increases in ISI lead to increases in P, which completes the upward slope of the masking curve. Figure 4A shows a u-shaped masking curve generated by this system (details of simulations are in the appendix). The mechanisms underlying this curve will be shown to be a variation of mask-blocking.

The drop in the masking curve as ISI increases can be understood by looking at the curves in Figure 4B, which plot $x(t)$ as a function of time for three ISIs. For the ISI=0 curve, $\tau_2 = 0$ and the mask has no effect on the decay of $x(t)$ because the masking ratio in equation (12) equals one ($I = J$ in these simulations). Since any effect of the mask is only at its onset, $x(t)$ is unchanged from a no-masking condition. This is very strong mask-blocking for the shortest ISI. For the ISI=50 condition, the masking ratio is less than one because $x(t)$ has undergone decay during the ISI period; as a result $x(\tau_1 + \tau_2)$ drops discontinuously to a fraction of its original value. Thus, the mask is not blocked as effectively by the target signal, and the downward slope of the u-shaped masking curve is formed. However, the system is slightly more complicated in that the effect of the mask also causes the rate of subsequent decay to decrease and the ISI=50 curve eventually is above the ISI=0 curve. In net, though, increasing the ISI from 0 to 50 produces release from mask-blocking, and that release has a bigger effect than the slower rate of decay. So P drops as the ISI increases from 0 to 50.

As ISI increases from 50 to 100, the VRF undergoes further decay during the ISI period. This produces several effects. First, the masking ratio becomes smaller, which implies that the mask has a bigger effect. Second, the magnitude of the discontinuous drop in $x(t)$ at mask onset is smaller and occurs later than for the ISI=50 condition; and this smaller and later drop tends to increase P relative to the ISI=50 condition. Second, the later appearance of the mask means that the slower rate of decay is also introduced later; and this tends to decrease P relative to the ISI=50 condition. Thus, there are two effects, one that promotes decreases in P and another that promotes increases in P. For the simulation parameters used here, the second term has the bigger effect, so P continues to drop as ISI increases from 50 to 100. For longer ISIs, the change in rate of decay has little effect and the later arrival of the discontinuous drop in $x(t)$ explains why P increases with ISI.

Further analysis indicates that the primary basis of the u-shaped masking function in the Anbar and Anbar model is a variation of mask-blocking, and that the mask-induced changes in rate of decay have only a secondary and coincidental effect. To support this claim, additional simulations were run that

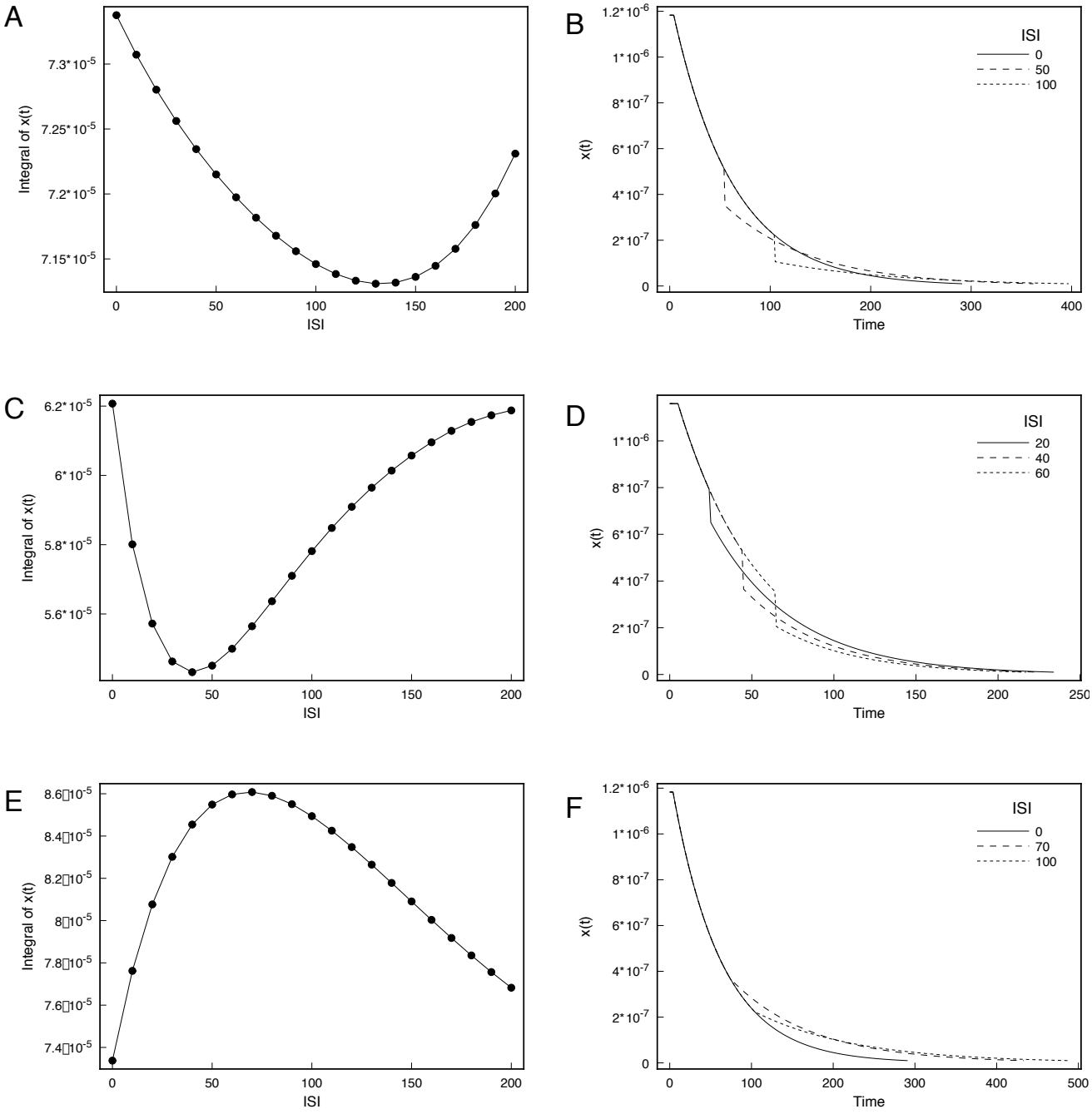

Figure 4: Simulations for Anbar and Anbar's (1982) model. A shows a u-shaped masking curve that replicates their original finding. B plots $x(t)$ for three SOAs and shows the effect of the discontinuous drop in $x(t)$ and the effect of changing the rate of decay at mask onset. C plots the u-shaped curve that results from fixing the rate of decay to be 0.02. D plots $x(t)$ for three SOAs that shows the effect of the discontinuous drop in $x(t)$. The rate of decay is fixed to be 0.02 in these calculations. E shows the masking curve that results from not applying the discontinuous drop in $x(t)$, but allowing the mask to change the rate of decay. F plots $x(t)$ for three SOAs and shows the mask's effect of changing the rate of decay at mask onset.

isolated the effect of the discontinuous drop in $x(t)$ at mask onset and the effect of changing the rate of decay. Figure 4C shows the masking curve generated when the rate of exponential decay was fixed at 0.02. The masking curve is still u-shaped, which indicates that the changes in decay are not crucial for generating the u-shaped masking curve. With the decay rate fixed it becomes clear that the Anbar and Anbar model accounts for the u-shaped masking curve because of mask-blocking. As ISI increases, the effect of the mask becomes stronger because $x(t)$ is smaller when the mask appears and the masking ratio becomes smaller. For strong enough $x(t)$ the masking effect is able to offset the fact that masking comes later (compare curves for ISI=20 and ISI=40 in Figure 4D). Eventually, though, the change in the immediate effect of the mask asymptotes because $x(t)$ is not so different between masks with ISIs of 40 and 60. Since the mask comes later with the larger ISI (Figure 4D), the masking curve increases.

Additional simulation results in Figures 4E and F show that removing the discontinuous drop in $x(t)$ due to mask onset and keeping the change in the rate of decay leads to a very different masking curve. As ISI increases from zero, the masking curve rises due to the slower decay introduced by the onset of the mask. Eventually, the later arrival of the slow decay stops being as effective because $x(t)$ is too small for the slower decay to contribute very much to P (compare the curves for ISI = 70 and 100 in Figure 4F). When the effect of changing the rate of decay is combined with the mask-blocking effects, the downward slope of the masking curve in Figure 4E can cause the bottom of the u-shaped masking curve in Figure 4C to shift to the right, as in Figure 4A. This is largely a coincidence of the particular model parameters and stimulus properties selected for this set of simulations.

The bottom line is that the u-shaped masking curve is the result of a type of mask-blocking. A strong target VRF weakens the effectiveness of the mask; in this case by producing a masking ratio close to one. As ISI increases, the target VRF decays in strength, so the mask ratio becomes smaller and the mask has a bigger effect. This is the basis of the decreasing part of the u-shaped masking curve. Eventually, the mask arrives too late to have much effect on the percept, and the masking curve rises again for larger ISIs.

Bridgeman's recurrent lateral inhibition simulations

Bridgeman (1971) proposed a seemingly very different model of metacontrast masking, which was subsequently refined in Bridgeman (1977, 1978). This model considers interactions of a single layer of neurons with recurrent lateral inhibition. Because the model includes a time delay as inhibition travels from one neuron to another, and the delay increases with spatial separation of neighboring cells, the network produces oscillatory responses. Moreover, a stimulus that initially feeds into only a few cells can produce variations in activity across large portions of the network. Each cell, i, in the network has an activity, $x_i(t)$, which is calculated by the equation:

$$x_i(t) = \left[I_i(t) - \sum_{k=-3,k\neq 0}^{3} w_{|k|} x_{i+k}(t-|k|) + SG_i(t) \right]^+ . \quad (13)$$

Here, $I_i(t)$ corresponds to input from various stimuli. The summation indicates lateral inhibition from nearby cells, with a time delay added to cells that are further away. $G_i(t)$ is a number randomly chosen from a standard normal distribution. S is a parameter that scales the random value. The notation $[\ ]^+$ indicates a nonlinearity so that if the terms inside are negative, $x_i(t)$ is set equal to zero.

Bridgeman suggested that the full pattern of activity across the network, rather than the behavior of just those cells stimulated directly by the input, is responsible for producing the visual percept. To measure masking effects, Bridgeman compared two spatio-temporal responses of the network: first without a mask, and second with a mask. To make the comparison, Bridgeman (1978) calculated, at every time step, the squared spatial correlation of cell activities. These squared correlations were then averaged over time and this average was taken as the relative strength of the target percept. Figure 5A plots the squared correlation as a function of time (each iteration corresponds to roughly 30 milliseconds) when the correlation is between two runs of the target alone (no mask). The correlation drops toward zero as time progresses because the target signal gradually drops below the level of the random noise inputs. The average height of this curve corresponds to the strength of the target percept. The curve essentially replicates simulations in Bridgeman (1978). Details of the current simulations are provided in the appendix.

To simulate metacontrast masking, one presents a target stimulus at some set of localized cells and then presents a mask stimulus at nearby flanking cells after an appropriate delay. Figure 5B shows that the average squared correlation value decreases as SOA increases up to two iterations (roughly 60 simulated milliseconds). This is the basic u-shaped masking curve.

Parts of Bridgeman's model seems quite consistent with the earlier analyses. In particular, the squared correlation is a VRF that decreases over time, and the strength of the target percept is the average (which is just a rescaling of the integral for these simulations) of this VRF. Indeed, much of the model's behavior can be described as mask-blocking, although this only becomes clear when the quantitative basis of the system is understood by other terms.

To see how the u-shaped masking curve comes about in Bridgeman's model consider a situation where the network activities behave in a linear fashion and the noise term is ignored ($S = 0$). If stimuli are chosen properly (e.g., the background luminance is large enough), the nonlinearity in equation (13) never applies. For such stimuli the network activities act in a linear fashion, so that the activities generated by a joint target and mask trial are equal to the sum of activities generated by separate target and mask trials. Consider two separate simulations, one where the target is presented alone and another where the mask is presented alone. The correlation between a metacontrast masking trial and target alone trial can be found

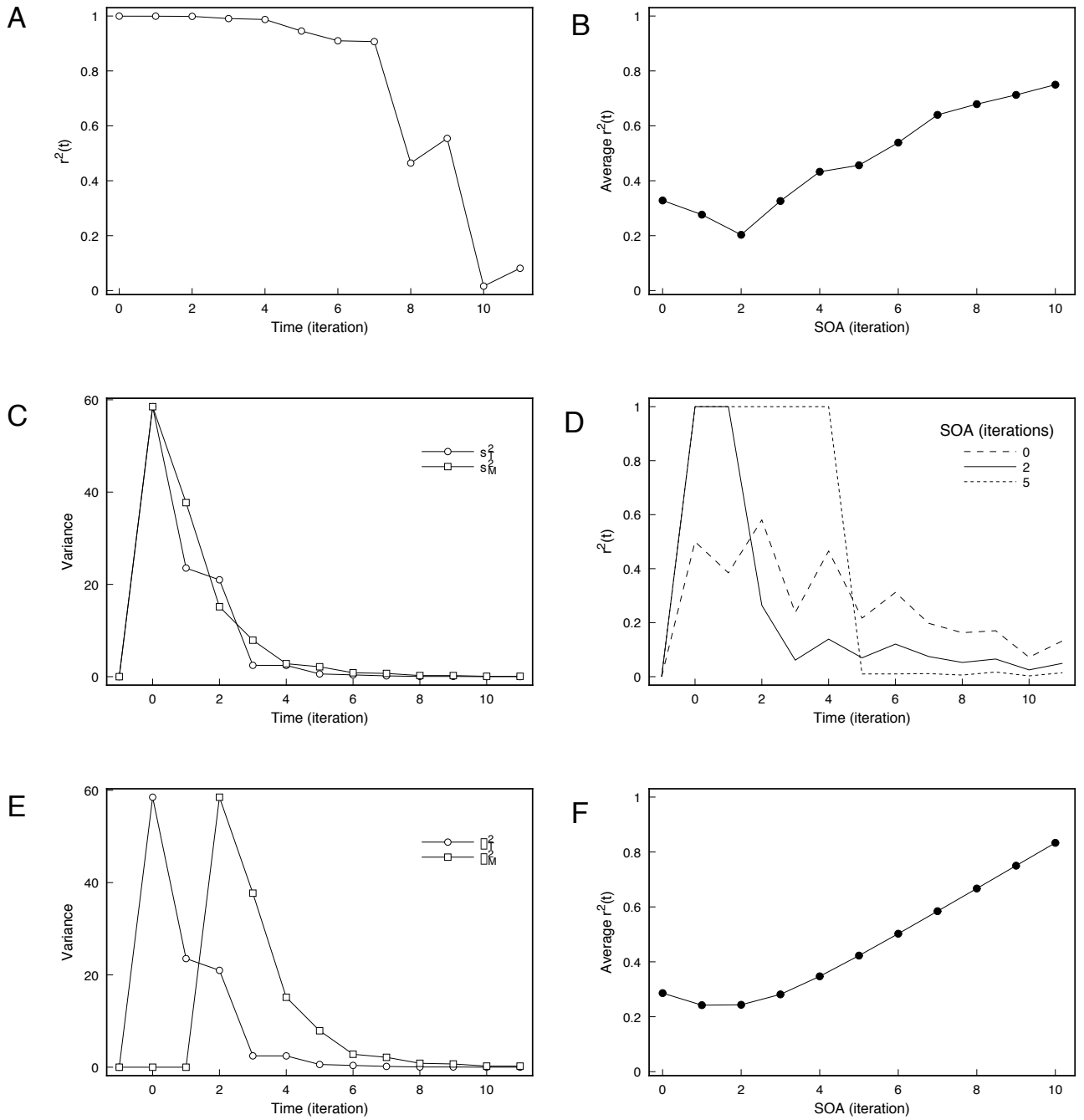

Figure 5: Simulations for Bridgeman's (1978) model. A plots the squared correlation as a function of time for two runs of target only presentations. The squared correlation gradually decreases because of noise added at each cell and iteration. B shows a u-shaped masking curve that replicates Bridgeman's basic finding. C plots variances for target-alone and mask-alone simulations as a function of time for SOA=0. The curves overlap substantially, thereby allowing mask-blocking to occur. D plots the squared correlation values for three SOAs as a function of time. E plots variances for target-alone and mask-alone simulations as a function of time for SOA=2. Because the mask variance does not overlap as much with the target variance, its masking effect is stronger than in C. F shows a u-shaped masking curve with r^2 calculated using equation (15).

by measuring the correlation between the activities in the target alone simulation and the sum of target and mask activities in the separate trials. By rewriting the correlation in terms of variances one finds that the squared correlation between the metacontrast trial and the target alone trial at time (iteration) t can be written as:

$$r^2(t) = 1 - \frac{\sigma_M^2(t)\left[1 - r_{TM}^2(t)\right]}{\sigma_T^2(t) + \sigma_M^2(t) + 2\sigma_T(t)\sigma_M(t)r_{TM}(t)}. \qquad (14)$$

Here $\sigma_T^2(t)$ is the variance across cell activities for the target only simulation at time t, $\sigma_M^2(t)$ is the variance across cell activities for the mask only simulation at time t, and $r_{TM}(t)$ is the correlation between cells in the separate target and mask simulations at time t. The derivation of equation (14) is provided in the appendix.

Again to help simplify the analysis, suppose that $r_{TM}(t) = 0$. Then equation (14) reduces to

$$r^2(t) = 1 - \frac{\sigma_M^2(t)}{\sigma_T^2(t) + \sigma_M^2(t)} = \frac{\sigma_T^2(t)}{\sigma_T^2(t) + \sigma_M^2(t)}. \qquad (15)$$

Thus, the squared correlation at a given time is the ratio of target variance and the sum of target and mask variances. The effect of the mask is to make this ratio smaller by making the denominator larger. If the target variance is much larger than the mask variance, the squared correlation is nearly one. If the target variance is small compared to the mask variance, the squared correlation is near zero. Thus, the mask has a weak effect when the target variance is large. A strong target signal *blocks* the mask signal.

Figure 5C plots $\sigma_T^2(t)$ and $\sigma_M^2(t)$ as a function of time for SOA=0. The variance curves overlap substantially, and spike to their largest value when the target/mask stimulus is first presented. The variance curves then decrease as neural activity is distributed across all the cells of the network. For the particular stimuli used in this simulation, $\sigma_M^2(t)$ is slightly larger than $\sigma_T^2(t)$ much of the time. As a result, $r^2(t)$ is generally less than 0.5, and grows smaller over time as Figure 5D shows. For the SOA=0 curve, the decrease in $r^2(t)$ over time occurs because $\sigma_T^2(t)$ decreases slightly faster than $\sigma_M^2(t)$, thereby causing the ratio in (15) to get smaller over time.

Figure 5E plots the variance curves with an SOA=2 and Figure 5D plots the corresponding $r^2(t)$ curve. Since the mask stimulus is presented at time 2, the mask variance is zero for smaller times, and $r^2(t)$ equals one. When the mask appears, its variance term spikes and then decreases as the mask activity spreads throughout the network. When the mask variance spikes, the target variance has already decreased because the network equations act to distribute the target's activity across cells. As a result, the peak of the mask variance term coincides with a relatively weak part of the target variance term and the effect on the calculation of squared correlation in equation (15) is substantial. In comparing the $r^2(t)$ curves for SOAs of 0 and 2, the sum of squared correlation is smaller for the SOA=2 curve because the strong masking late in the curve offsets the freedom from masking before the mask arrives early in the curve. The net effect is that the average squared correlation drops as SOA increases from 0 to 2, as in Figure 5F.

When analyzed in terms of target and mask variances and their contributions to squared correlation, the u-shaped masking curve is seen to be a variation of mask-blocking. When the target variance is strong, the effect generated by the mask is weak. The overlap of strong target variance with the mask variance decreases as SOA increases, so up to a point, increases in SOA lead to stronger masking. For long SOAs, the change in target variance at time of mask onset is minor and mask-blocking is weak. As a result, the squared correlation increases with SOA because the mask's effect comes later. Figure 5D is analogous to Figures 2B and 4B although the mechanisms and interpretation of components are dramatically different.

There are other characteristics of Bridgeman's model that complicate the story somewhat. The above analysis assumes that $r_{TM}(t) = 0$, which is not generally true. In the current simulations this correlation varied between ± 0.5, starting with a negative value and generally increasing toward a positive value. These changes affect the values of points on the masking curve, but the curve retains its u-shape. In additional simulations $r_{TM}(t)$ was replaced with random variables between ± 0.5 and the masking curve still showed the u-shape. Likewise, including the noise term at every iteration of the network generally makes only minor changes in the overall shape of the masking curve. Figure 5B is the masking curve with the noise and proper $r_{TM}(t)$ used. Finally, if stimulus conditions are set so that the nonlinearity in equation (13) does apply, the masking curve will again deviate somewhat from the above analysis, but the u-shaped curve still is generated.

This analysis also highlights which properties of the model are important for its account of metacontrast properties. For example, it does not seem to be significant that there is a temporal delay as neural activity spreads from one cell to another. Nothing in the calculation of variance depends strongly on the characteristics of delay. Likewise, the oscillatory responses in the model do not seem to be crucial for producing the u-shaped masking curve. As another example, model simulations in Bridgeman (1978) correctly showed that masking becomes weaker as the target and mask stimuli are separated in space. Given that the calculation of target variance and mask variance do not depend on the location of their respective stimuli in space, we can conclude that the effects of separation must be influencing $r_{TM}(t)$. A similar analysis can be applied to other simulations to identify how they influence equation (15) and the overall masking effects. More generally, it is clear that the u-shaped masking curve is a robust property of this model, because it depends on mask-blocking, which is easily generated.

Francis' Boundary Contour System simulations

Francis (1997) simulated a neural network model called the Boundary Contour System (BCS), which was originally proposed by Grossberg and Mingolla (1985a,b) to account for properties of spatial vision. The network is a complicated one, with multiple levels, specific receptive field shapes, lateral inhibition, cross-orientational inhibition, excitatory feedback, and inhibitory feedback. A full simulation involved simultaneous integration of nearly 40,000 differential equations through hun-

dreds of time steps.

As Francis described the model's behavior, the u-shaped masking curve arose from interactions between excitatory feedback generated by the target and feedforward inhibition generated by the mask. The excitatory feedback results in long-lasting persistence of signals corresponding to the target (Francis, Grossberg & Mingolla, 1994), but the strength of the feedback weakens as the feedback signals slowly fade away [the precise mechanisms are complicated and described in Francis *et al.* (1994)]. If the inhibitory signal from the mask arrives when the excitatory feedback is strong (e.g., short SOA or ISI), then the inhibition has little effect. If the mask arrives when the excitatory feedback is weaker, then the mask can curtail the remaining persisting signal. If the mask arrives much later, it is too late to have much of an effect. In Francis' simulations, the percept strength was measured as the duration of target responses above a threshold (equations 4 and 5), and Figure 6A plots the percept strength as a function of SOA. Simulation details are in the appendix.

Francis' verbal description of network interactions is essentially a description of mask-blocking, although other factors also play a role. The excitatory feedback in the BCS effectively lengthens the duration of the target signal, and the mask's inhibitory signal is too weak to have much effect when the target (or the feedback) is present. Figure 6B shows this interaction by plotting the activity of the model's VRF against time. In this model the VRF is the largest cell activity that is generated by the target. When this activity drops below a threshold, the activity of the target has effectively vanished from the network. The target percept strength is the time spent above the threshold. Three curves are shown with SOAs of 0, 40 and 80 milliseconds. In all conditions, the VRF remains strong well beyond the offset of the target (16 milliseconds) because of the excitatory feedback. The VRF also peaks after target offset because there is a slight time lapse before the strong excitatory feedback contributes to the measured cells.

Figure 6B is analogous to Figures 2B, 4D, and 5D, which demonstrate mask-blocking. In figure 6B, the SOA=0 curve shows weak masking at short times, as indicated by its being slightly below the other curves. The overall masking effect is stronger for the SOA=40 curve, which exhibits the influence of the mask after approximately time 50 (there is a short delay before the inhibitory signal from the mask reaches the appropriate level of the neural network). Masking with SOA=80 is stronger still, as is indicated at approximately time 90 where the SOA=80 curve branches down from the SOA=40 curve.

Francis (1997) related percept strength to the duration of the target-generated signals, with a variation of equations (4) and (5) above, so it is possible that the properties of efficient masking also apply here. Because of the complexity of the model it is difficult to disentangle the effects of mask-blocking from any effects related to efficient masking. However, Figure 6C demonstrates a similarly shaped masking curve for the integral of the VRF (equation 9). Given that the bottom of each masking curve is around SOA=70, and that efficient masking is unlikely to apply in Figure 6C because of Theorem 2, it seems probable that efficient masking has only a small effect on the u-shaped

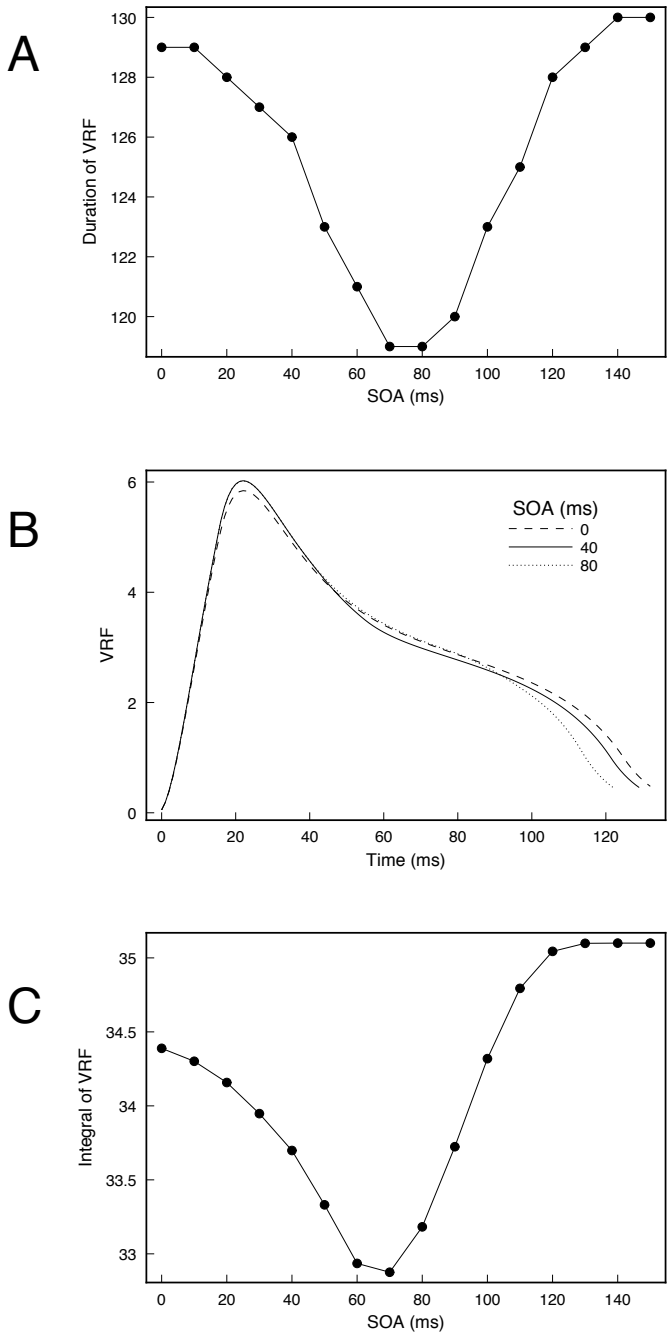

Figure 6: Simulation results for Francis's (1997) BCS model. A shows a u-shaped masking curve when the percept strength is measured as duration of the VRF. B plots the visual response function plotted against time for three different SOAs. C shows the u-shaped masking curve when percept strength is measured as integration of the VRF signal.

masking curve in Figure 6A.

In short, despite its complexity, the BCS system's dynamics account for the u-shaped masking curve with a variation of mask-blocking. One should not conclude that the BCS' complexity is unnecessary, though, as the BCS has been used to account for a variety of other properties of visual perception that would otherwise seem to have little to do with metacontrast masking (e.g., Grossberg, 1994). One of the strengths of this theory is that its components were designed to accommodate entirely different data sets.

Weisstein's transient-sustained simulations

Weisstein (1968, 1972) elaborated on an idea in Landahl (1967) to show that a system of differential equations could produce metacontrast masking if one designed the equations so that the inhibitory signal from the mask was faster and more transient than the excitatory signal generated by the target. The model was described as two pathways of neurons; one for the target signal and one for the inhibitory signal from the mask. Weisstein quantified this idea with a simple network of five neurons (three in the target excitatory path and two in the inhibitory path). Figure 7A schematizes the neurons in this model. This was not meant to be a formal model of the cellular basis of metacontrast masking, but one simple system that demonstrated the effect.

As Weisstein described the model, since inhibition develops at a faster rate than excitation, and masking is strongest when the inhibitory signal from the mask overlaps with the excitatory signal from the target, the mask should be delayed relative to the target, else the inhibition comes and goes before excitation begins. This verbal description suggests that target-blocking is the basis for the u-shaped masking curve in this system. As it turns out, this description is incomplete, and mask-blocking also plays an important role.

In setting out to replicate Weisstein's simulations, it was discovered that there are a few discrepancies in the model description. First, there seems to be an error in the description of the inhibition coming into the third cell ($3T$) in the target pathway. The apparent correction is given in the appendix of this paper. Second, it is unclear exactly how Weisstein measured the target percept. In many places in the text Weisstein (1968, 1972) proposed to measure percept strength as the "maximum cumulative frequency of firing" of cell $3T$. It is not clear what this means. Because firing frequency cannot become negative, the maximum cumulative frequency is the same thing as the cumulative frequency at time infinity. After playing with a simulation and gleaning information from Weisstein's graphs, it seems that for some simulations she actually measured the target percept as the maximum frequency of firing for cell $3T$. If we run the simulation this way, we get the masking curve in Figure 7B, which is quite similar to one found by Weisstein (1968, Figure 2). While there are minor differences, the new simulation basically verifies Weisstein's original findings.

Moreover, it seems that the underlying computational basis for the behavior of the network is accurately portrayed by Weisstein's verbal discussion and is an example of target-blocking. The relative timing of the target and mask signals matters the most because the maximum response at the third target cell will be smallest if the inhibitory signal from the mask directly overlaps with the target excitation feeding into that cell. Figure 7C shows the excitatory and inhibitory inputs feeding into cell $3T$ as a function of time for three different SOAs. The net input into cell $3T$ is the excitatory value minus the inhibitory value at each moment in time. As SOA changes, the timing of the inhibitory input varies. For SOA=0 much of the fast acting inhibitory input grows and disappears before the excitatory input arrives. As a result, the excitatory input to cell $3T$ is quite strong, and the cell reaches a large peak response. When the mask is delayed for an SOA of 70 milliseconds, the inhibition overlaps strongly with the excitation, so the net input to cell $3T$ is weaker than before. As a result, cell $3T$'s peak activity is smaller. When the mask is delayed for an SOA of 120 milliseconds, the inhibition arrives when the excitation is fading, so the masking effect on cell $3T$ is less than it was for an SOA of 70. These target-blocking effects are made clear in Figure 7D where the peak activity of cell $3T$ can be easily found for different SOAs.

However, there are problems. Elsewhere in Weisstein (1968), and explicitly in Weisstein (1972, pp. 248–249), it is stated that the measurement of target percept strength is the integral of activity from the third cell in the target pathway. Moreover, it seems that this was the method used for fits of the model to various psychophysical data. This leads to an additional problem. The calculation of the integral as defined by Weisstein is inconsistent with her verbal description of the model. In any simulation where the equations cannot be solved analytically, the integral is not really taken to positive infinity, but to some large time where the term to be integrated is negligible. In her simulations Weisstein set this large time to be 400 simulated milliseconds after onset of the target. As it turns out, the choice of integration range has a big effect on the shape of the masking curve.

Figure 7E shows two masking curves. One curve, *To time 400*, corresponds to the integration method used by Weisstein (1972), which was integration of cell $3T$ activity from time zero to time 400. The other curve, *To negligible*, corresponds to a new simulation where the integral was taken up to a time where the activity of cell $3T$ reached some negligible value. This time varies from one masking situation to another. The two curves are strikingly different, with the *To negligible* curve flattening out for SOAs between 70 and 170 ms. At SOAs beyond 180 milliseconds both integrals are identical.

For the cell parameters used by Weisstein, the response of cell $3T$ outlasts the inhibition generated by the mask (note the time scale difference between Figures 7C and D). As a result, after the inhibitory signal from the mask disappears, the integral of cell $3T$'s activity continues to contribute to the total integral. By stopping the integral at time 400, Weisstein inadvertently ignored these contributions. The curve in Figure 7E marked as *To time 400* starts to increase for SOAs beyond 70 milliseconds because there is less overlap between the excitation and inhibition feeding into cell $3T$ (as in Figure 7C). As a result, input to cell $3T$ is freed from target-blocking and the activity of cell $3T$ is bigger and the resulting integral is larger. However, the

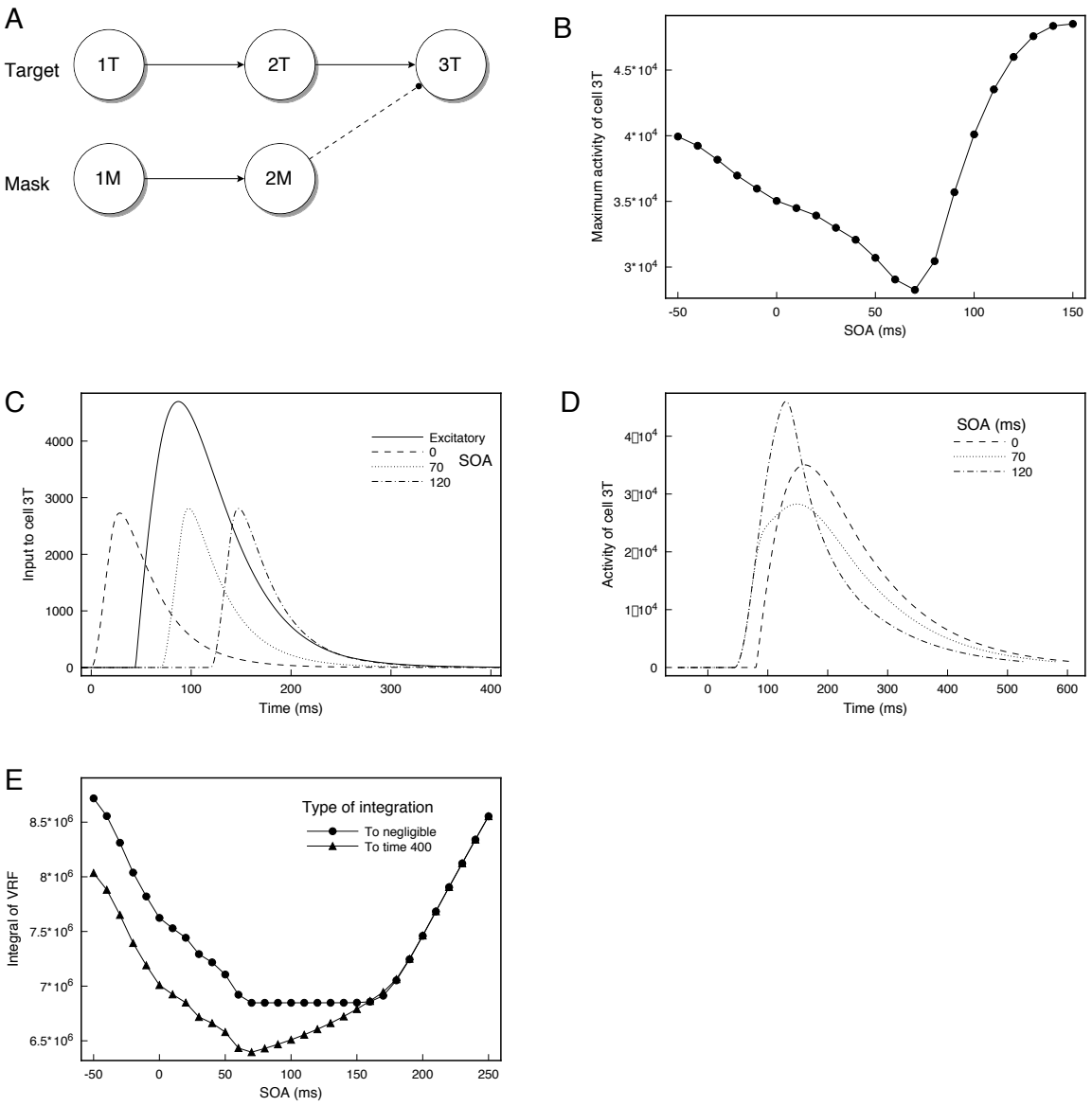

Figure 7: Simulation results for Weisstein's (1968, 1972) model. A schematizes the cells and connections in the model. The dashed line indicates inhibition from the mask. B shows a u-shaped masking curve that generally replicates a simulation in Weisstein (1968). C plots the inputs to cell $3T$ (one excitatory and three inhibitory) as a function of time, with the inhibitory input changing for different SOAs. Because of the delay in the creation of the excitatory input, the greatest overlap occurs when the mask is delayed by 70 milliseconds. D plots the activity of cell $3T$ as a function of time for three SOAs. E shows two u-shaped masking curves generated by taking the integral of cell $3T$ activity. The different shape of the curves is due to undermeasurement of the full integral by the *To time 400* method compared to the *To negligible* method.

delayed inhibition also means that the mask is present for a larger time without mask-blocking. This can be seen in Figure 7D where the curve for SOA=120 crosses below the curve for SOA=70. Thus, going from SOA=70 to SOA=120 has two effects on the integral. First, it causes release from target-blocking, which tends to increase the integral. Second, it causes release from mask-blocking, which tends to decrease the integral. By stopping the integral at time 400, Weisstein's simulations did not measure the full effect of the mask, so the target-blocking effect tends to dominate the value of the integral. Thus, the *To time 400* masking curve increases as SOA increases from 70 to 120.

However, when the full effect of the delayed inhibition is measured in the *To negligible* simulation, one sees that the increase in cell $3T$ activity due to release from target-blocking is nearly exactly offset by the release from mask-blocking when the mask arrives later. This explains why the *To negligible* curve in Figure 7E is flat between SOAs of 70 and 170. Weisstein's integration technique stopped too soon to add in the full effect of the mask. Mask-blocking also contributes to the downward slope of the curve for SOAs less than 70.

These new simulations clarify the results reported by Weisstein. First, the model can produce the u-shaped masking curve in a number of different ways, depending on how the cellular responses are related to percept strength, and depending on the range of integration of the cellular response. One could reasonably argue that the integration of cell $3T$ only occurs in 400 millisecond time periods. If one makes this assumption, then target-blocking is more important than mask-blocking, although both are present. However, it is not clear why 400 is more appropriate than 300 or 500 millisecond integration periods. Moreover, while reasonable, this specific integration period is not consistent with the verbal description Weisstein used in most of her discussion. When the model is analyzed in its intended spirit, one finds that target-blocking and mask-blocking effects are equally represented in the masking curve. This is a notable finding because Weisstein's simulation results are often taken as a quantitative version of the transient-sustained theories (e.g., Bischof & Di Lollo, 1995). At least as described verbally, the transient-sustained theories seem most similar to target-blocking interactions. However, Weisstein's simulations actually include both target-blocking and mask-blocking effects. It seems that Weisstein's original version of Figure 7B is the sole production of a u-shaped masking curve that uses *only* target-blocking interactions.

Conclusions

That masking strength should ever increase with ISI has always been the most notable characteristic of metacontrast masking, and seemingly was the most difficult property to explain. The current analysis demonstrates that this view is not correct. The u-shaped masking curve is a robust and general property of a number of systems, both simple and complex.

There are two main conclusions to be drawn from this study. First, there are at least three different methods to produce the u-shaped masking curve. One method is efficient masking, as described in Theorem 1. This method requires gradual decay of the target VRF and seems to require a particular linking hypothesis between the target signal and the percept. A second method is mask-blocking, whereby a strong target signal prevents the mask from having its effect. This method requires that lasting traces of the target be able to block the mask signal to insure that the strongest masking occurs for a positive ISI. The third method is target-blocking, where the mask signal prevents the target from producing a strong signal in the target VRF. This method requires time lags between the target and mask signals to insure that the strongest masking occurs for a positive ISI. The robustness of these methods indicates that a wide variety of models probably produce the u-shaped masking curve, but have never been explored for that purpose.

The second main conclusion is perhaps more notable: almost every previously published simulation of the u-shaped metacontrast masking curve has used mask-blocking. The single curve generated by Weisstein (1968), and reproduced in Figure 7B, is the only exception, and it was apparently not investigated further. Given the variety of options for generating the u-shaped curve, it is surprising that a common method is used in every model. It is also surprising because at a surface level the models seem dramatically different. It is not at all obvious that a model with thousands of differential equations and excitatory feedback (Francis, 1997) would account for masking in the same way as a model with a single differential equation and discontinuous masking effects (Anbar & Anbar, 1982). Likewise, it is interesting that both the Weisstein (1968, 1972) and Bridgeman (1971, 1977, 1978) models use a similar method to generate masking curves. Bridgeman's model was criticized by Weisstein, Ozog and Szoc (1975), yet the current analysis suggests that the models (at some level) are similar.

One should not conclude, however, that the four models are isomorphic. There are substantial and meaningful differences between the models and, although they use similar quantitative mechanisms, the physical mechanisms that would need to exist to generate the particular calculations of a given model differ greatly. Moreover, the current analysis has only explored the generation of the u-shaped masking curve. There are other properties of metacontrast masking that are related to the duration of the stimuli, the intensity of the stimuli, the spatial separation of the stimuli, and a variety of other factors. Many of these stimulus characteristics interact with the effects of ISI, and the models exhibit different results under some of these conditions. It will be important for future work to determine which masking properties can be accounted for with the model-free concepts of efficient masking, mask-blocking, and target-blocking. Only once these properties are understood can we determine if the components of a specific model add anything fundamentally new to an account of masking phenomena.

Two masking effects stand out as especially interesting. First, if a second mask is added to the standard metacontrast display, it can free the target from the effect of the first mask (e.g., Breitmeyer, Rudd & Dunn, 1981). This effect has only been quantitatively reproduced by Francis (1997), using mechanisms (inhibitory feedback) that elaborate the masking methods de-

scribed here. It would be very interesting to find a general quantitative description of this effect. Second, in the standard masking paradigm, the measurable effect of the mask varies with the observer's task. For example, even under conditions where observers report they do not see the target stimulus, studies find that reaction times to a target-mask pair are no slower than to the target alone presentation (e.g., Fehrer & Raab, 1962). Some of the effects of the observer's task have been accounted for by Bridgeman (1978) and Francis (1997) by hypothesizing that different tasks require different relationships between the measured percept strength and the VRF. As was already noted, the definition of this relationship has a large effect on masking curves, and further exploration along these lines should be illuminating.

Perhaps the most important observation from the current study is that since the u-shaped masking curve is so easily created in a number of different models, the field should generally conclude that there is nothing special about the u-shape of the masking curve. The u-shaped masking curve does not, by itself, impose a very strong constraint on the types of models that must be built to account for dynamic visual perception. A model that solely accounts for the u-shaped masking curve is of little interest. Comparisons between models need to be based on the models' ability to account for other properties of visual masking and visual perception in general.

References

Alpern, M. (1953). Metacontrast. *Journal of the Optical Society of America*, **43**, 648–657.

Anbar, S. & Anbar, D. (1982). Visual masking: A unified approach. *Perception*, **11**, 427–439.

Bachmann, T. (1994). *Psychophysiology of visual masking: The fine structure of conscious experience.* Commack, New York: Nova Science Publishers, Inc.

Bischof, W. F. & Di Lollo, V. (1995). Motion and metacontrast with simultaneous onset of stimuli. *Journal of the Optical Society of America, A*, **12**, 1623–1636.

Breitmeyer, B. (1978). Metacontrast masking as a function of mask energy. *Bulletin of the Psychonomic Society*, **12**, 50–52.

Breitmeyer, B. (1984). *Visual masking: An integrative approach.* New York: Oxford University Press.

Breitmeyer, B. & Ganz, L. (1976). Implications of sustained and transient channels for theories of visual pattern masking, saccadic suppression, and information processing. *Psychological Review*, **83**, 1–36.

Breitmeyer, B., Rudd, M. & Dunn, K. (1981). Metacontrast investigations of sustained-transient channel inhibitory interactions. *Journal of Experimental Psychology: Human Perception and Performance*, **7**, 770–779.

Bridgeman, B. (1971). Metacontrast and lateral inhibition. *Psychological Review*, **78**, 528–539.

Bridgeman, B. (1977). A correlational model applied to metacontrast: Reply to Weisstein, Ozog and Szoc. *Bulletin of the Psychonomical Society*, **10**, 85–88.

Bridgeman, B. (1978). Distributed sensory coding applied to simulations of iconic storage and metacontrast. *Bulletin of Mathematical Biology*, **40**, 605–623.

Busey, T. & Loftus, G. (1994). Sensory and cognitive components of visual information acquisition. *Psychological Review*, **101**, 446–469.

Dennett, D. (1992). Time and the observer: The where and when of consciousness in the brain. *Behavioral and Brain Sciences*, **15**, 183–247.

Di Lollo, V. & Bischof, W. (1995). Inverse-intensity effect in duration of visible persistence. *Psychological Bulletin*, **118**, 223–237.

Dixon, P. & Di Lollo, V. (1994). Beyond visible persistence: An alternative account of temporal integration and segregation in visual processing. *Cognitive Psychology*, **26**, 33–63.

Farrell, J., Pavel, M., & Sperling, G. (1990). The visible persistence of stimuli in stroboscopic motion. *Vision Research*, **30**, 921–936.

Fehrer. E. & Raab, D. (1962). Reaction time to stimuli masked by metacontrast. *Journal of Experimental Psychology*, **63**, 143–147.

Francis, G. (1997). Cortical dynamics of lateral inhibition: Metacontrast masking. *Psychological Review*, **104**, 572–594.

Francis, G. (1998). Metacontrast masking. In *Visual Perception Online Laboratory*, `http://www.psych.purdue.edu/~coglab/VisLab/`.

Francis, G. (1999). Spatial frequency and visual persistence: Cortical reset. *Spatial Vision*, **12**, 31–50.

Francis, G., Grossberg, S., & Mingolla, E. (1994). Cortical dynamics of feature binding and reset: Control of visual persistence. *Vision Research*, **34**, 1089–1104.

Gardner, M. (1961). *The 2nd Scientific American Book of Mathematical Puzzles & Diversions.* New York: Simon and Schuster.

Gaudiano, P. (1992). A unified neural model of spatiotemporal processing in X and Y retinal ganglion cells. *Biological Cybernetics*, **67**, 11–21.

Grossberg, S. (1980). How does the brain build a cognitive code? *Psychological Review*, **87**, 1–51.

Grossberg, S. (1983). The quantized geometry of visual space: The coherent computation of depth, form and lightness. *The Behavioral and Brain Sciences*, **6**, 625–657.

Grossberg, S. (1994). 3-D vision and figure-ground separation by visual cortex. *Perception & Psychophysics*, **55**, 48–120.

Grossberg, S. (1999). The link between brain learning, attention, and consciousness. *Consciousness and Cognition: An International Journal*, **8**, 1–44.

Grossberg, S. & Mingolla, E. (1985a). Neural dynamics of form perception: Boundary completion, illusory figures, and neon color spreading. *Psychological Review*, **92**, 173–211.

Grossberg, S. & Mingolla, E. (1985b). Neural dynamics of perceptual grouping: Textures, boundaries, and emergent segmentations. *Perception & Psychophysics*, **38**, 141–171.

Hildreth, J. D. (1973). Bloch's law and a temporal integration model for simple reaction time to light. *Perception & Psychophysics*, **14**, 421–432.

Kahneman, D. (1967). An onset-onset law for one case of apparent motion and metacontrast. *Perception & Psychophysics*, **2**, 577–584.

Landahl, H. D. (1967). A neural net model for masking phenomena. *Bulletin of Mathematical Biophysics*, **29**, 227–232.

Lefton, L. A. (1973). Metacontrast: A review. *Perception & Psychophysics*, **13**, 161–171.

Loftus, G. R., Duncan, J., & Gehrig, P. (1992). On the time course of perceptual information that results from a brief visual presentation. *Journal of Experimental Psychology: Human Perception and Performance*, **18**, 530–549.

Reeves, A. (1982). Metacontrast U-shaped functions derive from two monotonic processes. *Perception*, **11**, 415–426.

Sperling, G. & Sondhi, M. (1968). Model for visual luminance discrimination and flicker detection. *Journal of the Optical Society of America*, **58**, 1133-1145.

Weisstein, N. (1968). A Rashevsky-Landahl neural net: Simulation of metacontrast. *Psychological Review*, **75**, 494–521.

Weisstein, N. (1972). Metacontrast. In D. Jameson & L. Hurvich (Eds.) *Handbook of sensory physiology* (Vol. 7, No. 4, *Visual psychophysics*). Berlin: Springer-Verlag.

Weisstein, N., Ozog, G., & Szoc, R. (1975). A comparison and elaboration of two models of metacontrast. *Psychological Review*, **82**, 325–343.

Appendix

Proofs

Proof of Theorem 1:

Equation (1), with equations (2) and (3), is a piecewise linear first-order differential equation, and it can be analytically solved in parts. Assuming $x(0) = 0$, during target presence, $0 \le t < \tau_1$, the solution is

$$x(t) = \frac{BI}{A + CI}\left(1 - \exp[-(A + CI)t]\right). \tag{16}$$

During the ISI between target offset and mask onset ($\tau_1 \le t < \tau_1 + \tau_2$)

$$x(t) = x(\tau_1)\exp[-A(t - \tau_1)]. \tag{17}$$

During mask presence ($\tau_1 + \tau_2 \le t < \tau_1 + \tau_2 + \tau_3$), the solution is

$$x(t) = x(\tau_1 + \tau_2)\exp[-(A + EJ)(t - \tau_1 - \tau_2)] - \frac{DJ}{A + EJ}\left(1 - \exp[-(A + EJ)(t - \tau_1 - \tau_2)]\right). \tag{18}$$

After the mask ($t \ge \tau_1 + \tau_2 + \tau_3$), the solution is

$$x(t) = x(\tau_1 + \tau_2 + \tau_3)\exp[-A(t - \tau_1 - \tau_2 - \tau_3)]. \tag{19}$$

The integration to compute P can likewise be split into parts

$$P = \int_0^{\tau_1} F[x(t)]dt + \int_{\tau_1}^{\tau_1+\tau_2} F[x(t)]dt + \int_{\tau_1+\tau_2}^{\tau_1+\tau_2+\tau_3} F[x(t)]dt + \int_{\tau_1+\tau_2+\tau_3}^{T} F[x(t)]dt. \tag{20}$$

By the definition of $F[\ ]$ in equation (5) and the assumption that $F[x(\tau_1 + \tau_2 + \tau_3)] > 0$, each of the last three integrals is the duration of the integration, so this simplifies to

$$P = \int_0^{\tau_1} F[x(t)]dt + \tau_2 + \tau_3 + T - (\tau_1 + \tau_2 + \tau_3), \tag{21}$$

so that the partial derivative with respect to ISI, τ_2, becomes

$$\frac{\partial P}{\partial \tau_2} = 0 + 1 + 0 + \frac{\partial}{\partial \tau_2}T - 1. \tag{22}$$

Now to find the last differential, it is necessary to find T such that $x(T) = G$ for $T > \tau_1 + \tau_2 + \tau_3$. Substituting into equation (19) above gives

$$G = x(\tau_1 + \tau_2 + \tau_3)\exp[-A(T - \tau_1 - \tau_2 - \tau_3)]. \tag{23}$$

Solving for T gives

$$T = -\frac{1}{A}\ln[G] + \tau_1 + \tau_2 + \tau_3 + \frac{1}{A}\ln\left[x(\tau_1 + \tau_2 + \tau_3)\right]. \tag{24}$$

Plugging this into equation (22) and applying the chain rule gives

$$\frac{\partial P}{\partial \tau_2} = 1 + \frac{1}{A}\frac{1}{x(\tau_1 + \tau_2 + \tau_3)}\frac{\partial}{\partial \tau_2}x(\tau_1 + \tau_2 + \tau_3). \tag{25}$$

To find the remaining differential on the right hand side, use equations (17) and (18) to write $x(\tau_1 + \tau_2 + \tau_3)$ in terms of τ_2, and find that:

$$\frac{\partial x(\tau_1 + \tau_2 + \tau_3)}{\partial \tau_2} = Ax(\tau_1)\exp[-A\tau_2]\exp[-(A + EJ)\tau_3]. \tag{26}$$

Substituting this calculation into equation (25), dividing out the common A term, and noting that the remaining terms in the numerator make up half of equation (18) allows the following simplification:

$$\frac{\partial P}{\partial \tau_2} = 1 - \frac{x(\tau_1+\tau_2+\tau_3) + \frac{DJ}{A+EJ}\left(1-\exp[-(A+EJ)\tau_3]\right)}{x(\tau_1+\tau_2+\tau_3)} < 0, \tag{27}$$

where the inequality holds because the fraction must be bigger than one. This completes the proof.

Proof of Lemma 1:

By Theorem 1, the strongest masking occurs for ISI τ_2^* when $x(\tau_1+\tau_2^*+\tau_3) = G$. Using equation (18) set

$$G = x(\tau_1+\tau_2^*)\exp[-(A+EJ)(\tau_3)] - \frac{DJ}{A+EJ}\left(1-\exp[-(A+EJ)(\tau_3)]\right). \tag{28}$$

Using equation (17) to substitute for $x(\tau_1+\tau_2^*)$, and then simplifying, one gets

$$G + \frac{DJ}{A+EJ}\left(1-\exp[-(A+EJ)\tau_3]\right) = = x(\tau_1)\exp[-A\tau_2^*]\exp[-(A+EJ)\tau_3]. \tag{29}$$

Taking the natural logarithm of both sides and solving for τ_2^* gives

$$\tau_2^* = \frac{\ln[x(\tau_1)]}{A} - \frac{1}{A}\ln\left[G + \frac{DJ}{A+EJ}\left(1-\exp[-(A+EJ)\tau_3]\right)\right] - \frac{A+EJ}{A}\tau_3. \tag{30}$$

Plugging in for $x(\tau_1)$ with equation (16) gives the equation in the form presented in the Lemma 1 statement.

Lemma 2: Varying mask intensity

For the system defined in Theorem 1 and Lemma 1, the ISI for strongest masking, τ_2^*, shifts to smaller values as mask intensity increases:

$$\frac{\partial \tau_2^*}{\partial J} \le 0. \tag{31}$$

Proof: One could directly calculate the derivative, but there is little benefit in such an exercise. Simply note that the last term in equation (30) must decrease as J increases. Likewise, $DJ/(A+EJ)$ and $(1-\exp[-(A+EJ)\tau_3])$ are increasing functions of J, and the natural logarithm is an increasing function, so the second term, with its minus sign, must also decrease as J increases. The first term does not vary with J, thus τ_2^* decreases as J increases, thereby indicating that the strongest masking occurs for smaller ISIs.

Lemma 3: Varying mask duration

For the system defined in Theorem 1 and Lemma 1, the ISI for strongest masking, τ_2^*, shifts to smaller values as mask duration increases:

$$\frac{\partial \tau_2^*}{\partial \tau_3} \le 0. \tag{32}$$

Proof: The proof is of the same style as for Lemma 2. The second and third terms of equation (30) must decrease as τ_3 increases.

Proof of Theorem 2: As in Theorem 1, if $F[x(\tau_1+\tau_2+\tau_3)] = 0$, then increases in τ_2 cannot lead to a decrease in P. Thus, to complete the theorem, we need only suppose that $F[x(\tau_1+\tau_2+\tau_3)] > 0$; which implies that the VRF is above threshold at the offset of the mask.

The proof follows the same course as in Theorem 1, except the analysis beyond equation (20) needs to consider the new definition of $F[\ ]$. As before, P can be split into parts:

$$P = \int_0^{\tau_1} F[x(t)]dt + \int_{\tau_1}^{\tau_1+\tau_2} F[x(t)]dt + \int_{\tau_1+\tau_2}^{\tau_1+\tau_2+\tau_3} F[x(t)]dt + \int_{\tau_1+\tau_2+\tau_3}^{T} F[x(t)]dt. \tag{33}$$

By the definition of $F[\ ]$ in equation (9), and the assumption that $F[x(\tau_1+\tau_2+\tau_3)] > 0$ this becomes

$$P = \int_0^{\tau_1} F[x(t)]dt + \frac{x(\tau_1)}{A}\left(1-\exp[-A\tau_2]\right) - G\tau_2 + \frac{x(\tau_1+\tau_2)}{A+EJ}\left(1-\exp[-(A+EJ)\tau_3]\right) - \frac{DJ}{A+EJ}\left[\tau_3 - \frac{1}{A+EJ}\left(1-\exp[-(A+EJ)\tau_3]\right)\right] - G\tau_3 + \frac{x(\tau_1+\tau_2+\tau_3)}{A} - G(T-\tau_1-\tau_2-\tau_3) - \frac{G}{A}, \tag{34}$$

where T is as defined in equation (24). Calculating the partial derivative with respect to ISI, τ_2, gives

$$\frac{\partial P}{\partial \tau_2} = x(\tau_1)\exp[-A\tau_2] - G - \frac{A}{(A+EJ)}\left(1-\exp[-(A+EJ)\tau_3]\right)x(\tau_1)\exp[-A\tau_2] + \exp[-(A+EJ)\tau_3]x(\tau_1)\exp[-A\tau_2] + G\frac{x(\tau_1)\exp[-A\tau_2]\exp[-(A+EJ)\tau_3]}{x(\tau_1+\tau_2+\tau_3)}. \tag{35}$$

This can be rewritten as

$$\frac{\partial P}{\partial \tau_2} = x(\tau_1+\tau_2)\left(1-\frac{A}{A+EJ}\right) + G\left(\frac{x(\tau_1+\tau_2+\tau_3) + \frac{DJ}{A+EJ}\left(1-\exp[-(A+EJ)\tau_3]\right)}{x(\tau_1+\tau_2+\tau_3)} - 1\right) \ge 0, \tag{36}$$

which completes the proof.

Derivation of squared correlation for Bridgeman's (1978) model: The correlation between a target only simulation and a target and mask simulation is (dropping the t notation):

$$r = \frac{n\sum x_i z_i - \sum x_i \sum z_i}{\sqrt{[n\sum x_i^2 - (\sum x_i)^2][n\sum z_i^2 - (\sum z_i)^2]}}, \tag{37}$$

where x_i is the activity of the ith cell for the target only simulation and z_i is the activity of the ith cell for the target and mask simulation. Summations are across all the cells in the network. The denominator can be rewritten in terms of variances, and provided $S = 0$ and the nonlinearity in equation (13) never applies, the numerator can be rewritten to reflect that $z_i = x_i + y_i$, where y_i is the activity of cell i for a mask only simulation.

$$r = \frac{n\sum x_i(x_i + y_i) - \sum x_i \sum (x_i + y_i)}{\sqrt{n\sigma_x^2 n\sigma_z^2}}. \tag{38}$$

Expanding and simplifying produces

$$r = \frac{n\sum x_i^2 - (\sum x_i)^2 + n\sum x_i y_i - \sum x_i \sum y_i}{n\sigma_x\sigma_z}. \tag{39}$$

The first pair of terms in the numerator is $n\sigma_x^2$ and the second pair of terms is n times the covariance between x and y terms, which can be written as standard deviations and correlation to get

$$r = \frac{n\sigma_x^2 + n\sigma_x\sigma_y r_{xy}}{n\sigma_x\sigma_z}. \tag{40}$$

If σ_z^2 is written in terms of deviation scores, X_i and Y_i, then

$$\sigma_z^2 = \frac{\sum (X_i + Y_i)^2}{n} = \frac{\sum X_i^2 + 2\sum X_i Y_i + \sum Y_i^2}{n} =$$

$$\sigma_x^2 + 2\sigma_x\sigma_y r_{xy} + \sigma_y^2, \tag{41}$$

so plugging back into equation (40) and factoring out the common $n\sigma_x$ term gives

$$r = \frac{\sigma_x + \sigma_y r_{xy}}{\sqrt{\sigma_x^2 + 2\sigma_x\sigma_y r_{xy} + \sigma_y^2}}. \tag{42}$$

Squaring both sides gives

$$r^2 = \frac{\sigma_x^2 + 2\sigma_x\sigma_y r_{xy} + \sigma_y^2 r_{xy}^2}{\sigma_x^2 + 2\sigma_x\sigma_y r_{xy} + \sigma_y^2}, \tag{43}$$

which can be rewritten as

$$r^2 = 1 - \frac{\sigma_y^2(1 - r_{xy}^2)}{\sigma_x^2 + 2\sigma_x\sigma_y r_{xy} + \sigma_y^2}. \tag{44}$$

In equation (14), $\sigma_T = \sigma_x$, $\sigma_M = \sigma_y$, and $r_{TM} = r_{xy}$.

Simulations

Figures 2 and 3

The plots in Figures 2 and 3 were created by integrating equation (1) with Euler's method using a step size of 0.01. The results presented in Figure 2 are based on the following parameters: $A = 0.01$, $B = 1$, $C = 1$, $D = 0.00031$, $E = 0.002$, $G = 0.2$, $I = 10$, $J = 10$, $\tau_1 = 20$, and $\tau_3 = 20$. The parameters for the results presented in Figure 3 were the same, except $E = 5.0$.

Anbar and Anbar's model

The simulations of Anbar and Anbar's (1982) model used $\gamma = 0.3$, $p = 0.442857143$, $I = J = 0.000001183$, and stimulus durations of 5 time units. These parameters satisfy constraints identified by Anbar and Anbar for their equations to produce the u-shaped masking curve. Anbar and Anbar did not report the parameters in their simulations (except for $\gamma = 0.3$), and their data plots have no numerical values so there is no way to determine if these are the same parameters as in the original study. Nevertheless, the curves look similar and probably demonstrate the same basic effects.

Bridgeman's model

A ring of 30 cells was created, with nearby neighbors allowing interactions. Each cell activity obeyed equation (13). For all simulations $w_0 = 0$, $w_1 = 0.3$, $w_2 = 0.3$ and $w_3 = 0.1$. For Figures 5A and B, $S = 0.1$. For Figures 5C–F, $S = 0$ and the simulation artificially set $r_{TM}(t) = 0$ when calculating equation (15).

Before presenting any stimuli, a background luminance of $I_i(t) = 50$ was presented to all cells and the network equations were updated for 200 iterations. This resulted in a nonzero activity among the cells, which could not be calculated analytically. After the initialization period, a target stimulus with intensity 22.5 was added to the background luminance and presented to the middle two cells for two iterations. A mask stimulus of equal intensity and duration was presented to two cells flanking the target and separated from the target by one cell.

For Figure 5B, masking effects were measured by first presenting a target alone and recording the $x_i(t)$ values for 12 iterations after the target onset. The values were then also recorded for a presentation of the target and the mask. The correlation across cell activities, $r(t)$, was then calculated for every iteration. The average squared correlation across all twelve iterations was then taken as the strength of the target percept. For Figures 5C–F, the correlation $r(t)$ was calculated by generating separate simulations with the target alone and the mask alone and then using equation (15) to combine the variance terms from the simulations.

Francis' model

The simulation results reported here are based on the equations and parameters previously published in Francis (1997). The target and mask stimuli were as described there with simulated luminance values of 1.0 and durations of 16 simulated milliseconds.

Weisstein's model

Each cell contains two values (excitation and inhibition), which obey separate differential equations. The first cell in the target pathway (cell $1T$) receives input from the target stimulus:

$$\frac{de_{1T}}{dt} = A_{1T}I(t) - B_{1T}e_{1T} \tag{45}$$

$$\frac{dj_{1T}}{dt} = C_{1T}I(t) - D_{1T}j_{1T}.$$

Here A_{1T}, B_{1T}, C_{1T}, and D_{1T} are parameters. e_{1T} is the excitatory part of the cell's response and j_{1T} is the inhibitory part of the cell's response.

The second cell in the target pathway (cell $2T$) receives input (both excitation and inhibition) from cell $1T$:

$$\frac{de_{2T}}{dt} = A_{2T}[e_{1T} - j_{1T}]^+ - B_{2T}e_{2T} \tag{46}$$

$$\frac{dj_{2T}}{dt} = C_{2T}[e_{1T} - j_{1T}]^+ - D_{2T}j_{2T}.$$

The third cell in the target pathway (cell $3T$) receives input from cell $2T$ and inhibition from the mask pathway via cell $2M$:

$$\frac{de_{3T}}{dt} = A_{3T}[e_{2T} - j_{2T}]^+ - [j_{2M} - e_{2M}]^+ - B_{3T}e_{3T} \tag{47}$$

$$\frac{dj_{3T}}{dt} = C_{3T}[e_{2T} - j_{2T}]^+ - [j_{2M} - e_{2M}]^+ - D_{3T}j_{3T}.$$

The term $[j_{2M} - e_{2M}]^+$ is different from Weisstein's (1972) report of the equations. It was found, however, that when the e and j terms were switched as Weisstein suggested, that this term never took nonzero values. Since this term is the source of masking inhibition, it is necessary that it take nonzero values. An alternative would be to keep Weisstein's equations but switch the parameters for e_{2M} and j_{2M}.

The mask pathway consists of two cells ($1M$ and $2M$). The equations governing these cells are identical to those for $1T$ and $2T$ above, except each T would be replaced by M, $I(t)$ would be replaced by $J(t)$, and the corresponding parameters are different.

For the masking curve in Figure 7A, the target percept is measured as the peak value of $[e_{3T} - j_{3T}]^+$. For the curves in Figure 7D, the integral of this term was calculated. For the curve marked *To time 400*, the limits of the integral were 0 and 400. For the curve marked *To negligible*, the integral was taken from 0 to the time at which the value of $[e_{3T} - j_{3T}]^+$ equaled the value 1000. The maximum height of the VRF was nearly 40,000. The *To negligible* masking curve was essentially the same shape when the integral was taken from 0 to the time at which the value of $[e_{3T} - j_{3T}]^+$ equaled one.

Parameter values were the same as described in Weisstein (1972) and were: $A_{1T} = 1.5$, $B_{1T} = 0.025$, $C_{1T} = 1.5$, $D_{1T} = 0.1$, $A_{2T} = 1.2$, $B_{2T} = 0.03$, $C_{2T} = 2.4$, $D_{2T} = 0.09$, $A_{3T} = 0.2$, $B_{3T} = 0.009$, $C_{3T} = 0.0$, $D_{3T} = 0.0$, $A_{1M} = 1.5$, $B_{1M} = 0.025$, $C_{1M} = 1.5$, $D_{1M} = 0.1$, $A_{2M} = 1.6$, $B_{2M} = 0.03$, $C_{2M} = 6.4$, $D_{2M} = 0.6$.

For all simulations the target and mask luminances were 29.75, and each target and mask was presented for 20 simulated milliseconds. The target stimulus always started at time zero, and every e and j variable was initially set to the value zero.

The differential equations were integrated with Euler's method using a step size of 0.01.

Received March 31, 1999
Revision received November 14, 1999
Accepted January 4, 2000